4^{th} URSI AT-RASC, Gran Canaria, 19 – 24 May 2024

Focused Downlink Radiofrequency Electromagnetic Field Exposure at 26 GHz Using an Analytical Model

Hanne Herssens*(1), Arno Thielens(1)(2)
(1) Department of Information Technology, Ghent University, 9000 Ghent, Belgium, *email:hanne.herssens@ugent.be
(2) Photonics Initiative, the Advanced Science and Research Center, the Graduate Center of the City University of New York, 10031 New York, NY, USA

Abstract

Wireless telecommunication requires downlink (DL) data transmission from the network to the user equipment (UE) and vice versa. New technologies for DL transmission use focusing of radiofrequency (RF) electromagnetic fields (EMFs) at the UE. Therefore, the DL exposure focused at the UE is determined here. We consider a UE located next to the skin receiving at 26 GHz. At this frequency, the exposure will be limited to superficial tissues such as the skin, which is modeled using a multi-layered model. Using this model, the EMFs can be determined analytically. Focusing of the EMFs is achieved by applying maximum ratio transmission precoding. It is found that there is a minimum number of incident plane waves (> 10) needed to achieve an EMF hotspot at the UE. The exposure is quantified using the peak spatial absorbed power density at the surface of the model. The absorbed power density depends on the UE location and behaves periodically as a function of distance between the UE and the skin if focusing is achieved.

1 Introduction

The deployment of the 5th generation (5G) cellular mobile networks changes the radiofrequency electromagnetic field (RF-EMF) exposure compared to the legacy technologies (2G-4G). In 5G networks, the downlink (DL) data transmission occurs over beams directed at the user equipment (UE), so-called beamforming, or by constructive interference using excitation of multiple channels with precoded antenna array transmissions, leading to a focusing of the EMFs around the UE location [1, 2]. This is a result of the Multiple-Input-Multiple-Output (MIMO) technology that is used by the base stations (BS) [3]. This technology enables precoding, i.e., the controlling of the amplitudes and phases of the BS antennas such that constructive interference occurs at the intended receiver (UE). As a result of this, the RF-EMF exposure will be focused at the UE.

The majority of the 5G networks that are rolled out in the EU operate in the frequency band around 3.5 GHz. Our previous work also focused on this frequency [2]. A new frequency band of emerging 5G networks is a frequency band centered around 26 GHz (24-28 GHz). At these higher frequencies, the short penetration depth will lead to a superficial absorption of the EMFs. Therefore, the exposure will be limited to superficial tissues like the skin. It is no longer useful to use (a part of) a whole-body model, as was done at lower frequencies [1, 2]. Additionally, these whole-body models will lead to a high computational cost. An often used model at this frequency is a multi-layered skin model [4, 5]. The authors of [5] compare such a model with an anatomically accurate whole-body model. They found that at this frequency the EMF distribution inside the tissues differs in a non-negligible way between the two types of models. However, we assume that the precoding of the EMFs will make this difference in distribution less important, since the exposure in this case will be even more localized than with single plane wave exposure. Such a multi-layered skin model has more advantages compared to the whole-body models besides computational cost. The thickness of the different layers can more easily be varied and the far-field exposure of such a model can be calculated theoretically [6].

In this work, the DL exposure focused at the UE, so-called auto-induced DL (a-DL) exposure [7], is determined using an analytical model. The UE is located next to the skin and operates at 26 GHz. The outline is as follows. Section 2 explains the analytical model and precoding that is used. Section 3 describes the obtained results. Section 4 forms a conclusion.

2 Materials and Methods

2.1 Analytical Model

Figure 1 shows the multi-layered skin model exposed to an incident plane wave (E_0^+). The model consists of a skin (epidermis + dermis, $l_1 = 1.2$ mm), a fat ($l_2 = 4$ mm), and a muscle ($l_3 = \infty$) layer representing the wrist [4]. This case could occur e.g., when wearing a smartwatch. At 26 GHz, the stratum corneum has a negligible effect, therefore this is not included in the model [5]. The dielectric properties of the layers are taken from [8]. In the x- and y-direction all layers have infinite dimensions.

The electric field resulting from an obliquely incident plane

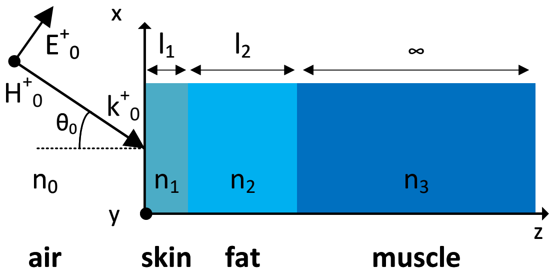

Figure 1. Multi-layered skin model consisting of a skin, fat and muscle layer exposed to an incident plane wave (E_0^+).

wave (E_0^+) under incidence angle θ_0 $[-\pi/2, \pi/2]$ is calculated [6]. Multiple reflections will occur at the tissue interfaces. The total electric field in each layer will thus be the sum of the incident and reflected fields in that layer. The muscle layer is assumed to be infinitely long such that there is no reflected wave in this layer. Using this and the boundary conditions, the total electric field can be calculated. Two polarizations of the incident field are considered in the calculations, i.e., TE (electric field perpendicular to xz-plane) and TM (electric field parallel to xz-plane). The electric field for any polarization angle ψ can then be obtained by

$$\mathbf{E} = sin(\psi)\mathbf{E}_{TE} + cos(\psi)\mathbf{E}_{TM}. \quad (1)$$

The same can be done for the magnetic field. The solutions of the electric and magnetic fields for any incidence angle θ_0 and any polarization angle ψ can then be used to determine the focused exposure discussed in the next section.

2.2 Focused Exposure

We assume that the base station is found in the far-field of the user, i.e., the incoming EMFs can be modelled as plane waves obtained in the previous section with an incident electric field strength $E_0^+ = 1\,\mathrm{V/m}$. Additionally, it is assumed that the plane waves can be incident from any direction, i.e., any θ_0 in Figure 1, and that the plane waves are randomly polarized. This study is limited to variations of the elevation angle and the azimuth angle is 0 such that the model is invariant along the y-direction. The focused exposure is obtained by ensuring that the incident plane waves will interfere constructively at the UE. A virtual UE is considered at different distances d from the skin ($x = 0, z = -d$ in Figure 1). Maximum ratio transmission precoding is used to focus the electric field to the location of the UE. This is done by controlling the phase and the amplitude of the individual plane waves [9]:

$$\mathbf{E}^{prec}(d,\mathbf{r}) = \sum_{l=0}^{N-1} \alpha(d) w_l(d) \mathbf{E}_l(\mathbf{r}) \quad (2)$$

$$w_l(d) = E_{i,l}^*(0,0,-d) \quad (3)$$

$$\alpha^2(d) \sum_{l=0}^{N-1} |w_l(d)|^2 = 1 \quad (4)$$

with $\mathbf{E}^{prec}(d,\mathbf{r})$ the precoded electric field at UE at $z = -d$, N the total number of incident plane waves, $\alpha(d)$ a normalization constant, $w_l(d)$ the precoding weight, $\mathbf{E}_l(\mathbf{r})$ the electric field obtained with plane wave l, and $E_{i,l}^*(0,0,-d)$ the complex conjugate of the ith-component of the electric field at UE at $z = -d$ obtained with plane wave l. The best component of the electric field, i.e., E_i in (3), to use for the precoding depends on the assumed polarization of the antenna in the UE. In this work, we have chosen to focus to an x-polarized UE. However, any random polarization could be studied in our approach. Note that, if the incident plane waves are TE-polarized, $E_x = E_z = 0$ and $E_y \neq 0$. If the incident plane waves are TM-polarized, $E_y = 0$ and, E_x and/or $E_z \neq 0$. An incident plane wave with a random polarization ψ, see (1), could thus induce any component E_x, E_y, or E_z.

At 26 GHz, the peak spatial absorbed power density (psS_{ab}) averaged over $4\,\mathrm{cm}^2$ is used to quantify the exposure [10]. At this frequency, the ICNIRP basic restriction is $20\,\mathrm{W/m}^2$. The absorbed power density is determined by:

$$S_{ab} = \frac{1}{A} \int_A \mathbf{S} \cdot \mathbf{n}\, dA \quad (5)$$

$$\mathbf{S} = \frac{\mathrm{Re}(\mathbf{E} \times \mathbf{H}^*)}{2} \quad (6)$$

with A the averaging area on the body surface ($z = 0\,\mathrm{cm}$) and $\mathbf{n}$ the unit vector normal to the averaging area. In this work, the EMFs will be invariant along the y-direction (Figure 1), therefore the power density $\mathbf{S}$ will be averaged along a line of 2 cm for $z = 0\,\mathrm{cm}$. The studied exposure situation consists of an UE located at a distance d from the skin. There are N incident plane waves with each a random incidence angle θ_0 and random polarization ψ.

3 Results

3.1 Focused Power Density

Figure 2 shows the power density flux focused at the UE (red circle) which is situated at a distance $d = 5\,\mathrm{mm}$ from the phantom for a different number of incident plane waves N. Each plane wave has a random incidence angle θ_0 and is randomly polarized. The maximum $|\mathbf{S}|$ is 7 dB, 13 dB and 15 dB higher than what is found for a single plane wave with $\theta_0 = 0$, $\psi = 0$ ($max(|\mathbf{S}|) = 0.73\,\mathrm{mW/m}^2$) with the same incident power density for $N = 10$, $N = 40$ and $N = 70$, respectively. For each N, the maximum power density is not found at the UE, but close to it, i.e., at $x = -2\,\mathrm{mm}$ and $z = -9\,\mathrm{mm}$, $x = 0\,\mathrm{mm}$ and $z = -3\,\mathrm{mm}$, and $x = 0\,\mathrm{mm}$ and $z = -3\,\mathrm{mm}$ for $N = 10$, 40, and 70, respectively. Note that for each configuration the precoding weights are normalized according to (4) such that each configuration has the same incident power density. For $N = 10$, the maximum $|\mathbf{S}|$ ($3.6\,\mathrm{mW/m}^2$) is much lower than in the other cases, i.e., $15.3\,\mathrm{mW/m}^2$ and $24.1\,\mathrm{mW/m}^2$ for $N = 40$ and 70, respectively. For $N > 10$, the precoding leads to a highly focused power density in the x-direction near the UE. The power density is less focused along the z-direction, since the incidence angles of the plane waves are limited to θ_0

$[-\pi/2, \pi/2]$. A higher N leads to a better focusing of the EMFs. The focusing effect is quantified by the full width at half maximum (FWHM) along the x-direction. For $N = 10$, the FWHM=∞, i.e., no hotspot of RF-EMF power density is formed. For $N = 40$, a hotspot is formed near the UE with FWHM=6 mm=0.52λ. Increasing N further to 70 leads to better focusing with FWHM=5 mm=0.43λ and a higher power density at the UE, i.e., 21.5 mW/m^2, compared to 13.7 mW/m^2 for $N = 40$. Future work consists of further quantifying the focus effect in terms of N.

3.2 Exposure Assessment

The white line at $z = 0$ in Figure 2 shows the averaging area for which the psS_{ab} is found. For the three cases, this area is centered along $x = 0$, i.e., along the same line as the focus point. This is not always the case. Figure 3 shows an example of this when $d = 10$ mm and $N = 70$. Figures 2 and 3 also show that the EMFs are mostly situated at the surface of the phantom ($z = 0$) and rapidly decrease for $z > 0$ as expected at 26 GHz, since the skin depth of human skin at this frequency is only 1 mm. The highest exposure will therefore be found at the surface.

The psS_{ab} is calculated for different distances of the focus point d for 100 samples when taking N random plane waves, i.e., 100 samples of N random values of θ_0 and ψ with θ_0 and ψ uniformly distributed between $-\pi/2$ and $\pi/2$, and 0 and 2π, respectively. The sample size is validated by repeating the procedure multiple times. Figure 4 shows the cumulative distribution function (cdf) of psS_{ab} for a different number of incident plane waves N. For $d = 30$ mm, the median values are $p_{50} = 0.77\,\text{mW/m}^2$ and $2.44\,\text{mW/m}^2$ using 10 and 70 plane waves, respectively. For $d = 5$ mm, the median values are $p_{50} = 0.97\,\text{mW/m}^2$ and $5.15\,\text{mW/m}^2$ using 10 and 70 plane waves, respectively. Figure 4 also shows the case for a single incident plane wave ($N = 1$). A lower exposure is found ($p_{50} = 0.29\,\text{mW/m}^2$), since no focusing can occur. A higher number of plane waves leads to a higher exposure for both locations of focus points. This is also in line with Figures 2 and 3 where higher fields were found with more incident plane waves leading to a higher power density along the surface of the skin. For $N = 70$, the psS_{ab} increases for decreasing distance of the focus point to the skin. This is expected since the power density will be concentrated at the focus point. Therefore a closer focus point will lead to higher fields at the surface. Using 10 plane waves, the distance of the focus point does not affect the psS_{ab}. Only using 10 plane waves does not lead to a focusing of EMFs. This was also seen in Figure 2a.

Figure 5 plots the psS_{ab} as a function of distance between the focus point and the phantom d for a different number of plane waves. The same configurations of plane waves as in Figure 2 are used. In general, the psS_{ab} decreases for increasing distance using $N = 40$ and $N = 70$. This behavior is not seen with $N = 10$. The distance of the focus point has almost no effect compared to $N = 40$ and $N = 70$. This is also an indication that no good focusing is achieved using only 10 plane waves. The psS_{ab} behaves periodically as a function of distance. The peaks are found at distances which are found at approximately half a wavelength apart ($\lambda/2 = 5.8$ mm). This also illustrates the focusing, since if a maximum power density is found near the focus point, local maxima will be found at distances $n\lambda/2$ from this point.

4 Conclusion

The a-DL exposure at 26 GHz focused at the UE located next to the skin is determined. The focusing of the EMFs using MRT precoding for a different number of incident plane waves is investigated. It is found that using only 10 plane waves does not lead to a good focusing of the EMFs, i.e., the FWHM=∞. The peak spatial absorbed power was determined as a function of the distance between the focus point and the skin. It was found that the psS_{ab} behaves periodically as a function of distance if enough plane waves are present to achieve a good focusing. Future work consists of normalizing the exposure to reference levels such that it can be compared with international guidelines. The thickness of the layers will also be varied, since a different thickness can result in a matched layer leading to a higher transmission of the EMFs. In this work random incidence of the plane waves is assumed. Channel measurements could be used as input to achieve a more realistic exposure. Future work also consists of extending this work to include the azimuthal angle and other UE polarizations.

5 Acknowledgements

This research was funded by the ETAIN project. The ETAIN project is funded by the European Union's Horizon Europe research and innovation funding program under grant agreement No. 101057216.

References

[1] S. Shikhantsov *et al.*, "Hybrid Ray-Tracing/FDTD Method for Human Exposure Evaluation of a Massive MIMO Technology in an Industrial Indoor Environment," *IEEE Access*, vol. 7, pp. 21 020–21 031, 2019.

[2] H. Herssens and A. Thielens, "Auto-Induced, Radiofrequency, Downlink Exposure Focused at the Human Ear," in *2023 53rd EuMC*, 2023, pp. 444–447.

[3] T. L. Marzetta, "Noncooperative Cellular Wireless with Unlimited Numbers of Base Station Antennas," *IEEE Trans. on Wireless Commun.*, vol. 9, no. 11, pp. 3590–3600, 2010.

[4] K. Sasaki, M. Mizuno, K. Wake, and S. Watanabe, "Monte Carlo simulations of skin exposure to electromagnetic field from 10 GHz to 1 THz," *Physics in Medicine & Biology*, vol. 62, no. 17, p. 6993, 2017.

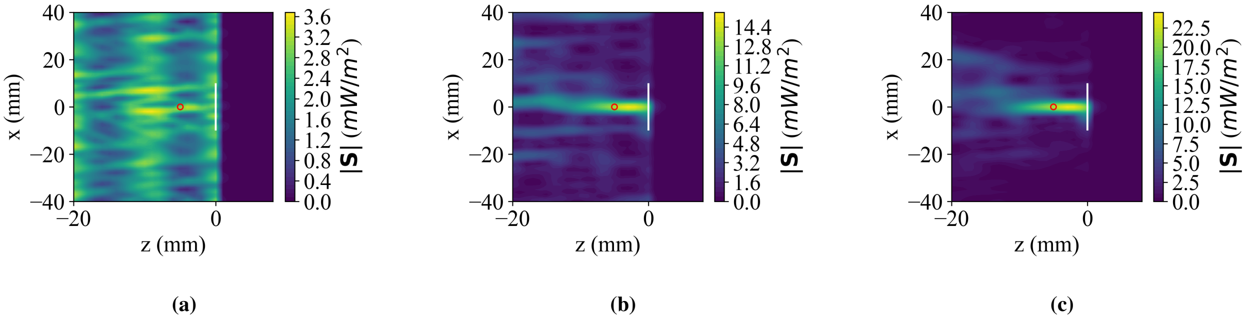

Figure 2. The power density focused at the UE (red circle, $d = 5\,\text{mm}$) with (a) $N = 10$. (b) $N = 40$. (c) $N = 70$. The precoding weights are normalized according to (4). The white line indicates the averaging area for which the *psSab* is found at the surface.

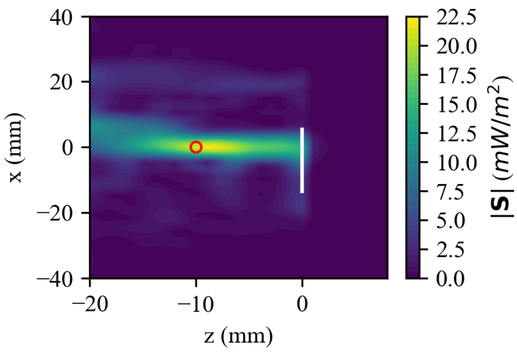

Figure 3. The power density focused at the UE (red circle, $d = 10\,\text{mm}$) with $N = 70$. The precoding weights are normalized according to (4). The white line indicates the averaging area for which the *psSab* is found at the surface.

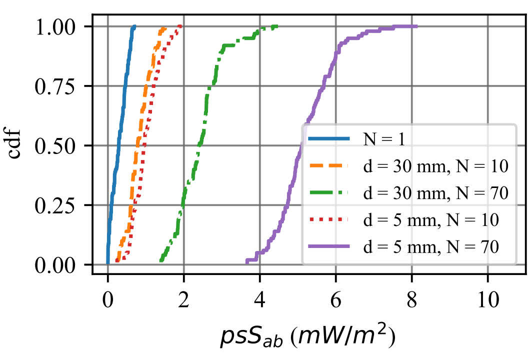

Figure 4. Cumulative distribution function (cdf) of psS_{ab} for a different number of plane waves N for different distances of the focus point d. The precoding weights are normalized according to (4).

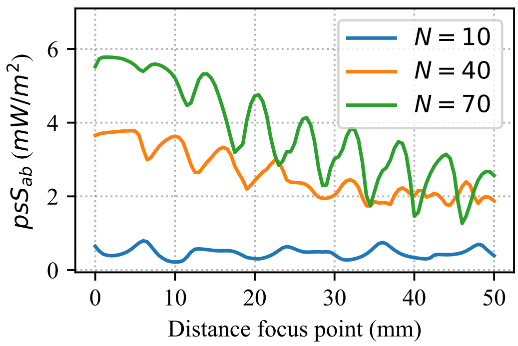

Figure 5. psS_{ab} as a function of distance of the focus point for a different number of plane waves sources N. The precoding weights are normalized according to (4).

[5] M. Colella *et al.*, "Advantages and Disadvantages of Computational Dosimetry Strategies in the Low mmW Range: Comparison Between Multilayer Slab and Anthropomorphic Models," *IEEE Trans. on Microw. Theory and Tech.*, vol. 71, no. 10, pp. 4533–4545, 2023.

[6] S. J. Orfanidis, "Electromagnetic waves and antennas," 2002.

[7] M. Velghe *et al.*, "Protocol for personal RF-EMF exposure measurement studies in 5th generation telecommunication networks," *Environmental Health*, vol. 20, no. 1, pp. 1–10, 2021.

[8] P. Hasgall *et al.*, "IT'IS Database for thermal and electromagnetic parameters of biological tissues, Version 4.0," *IT'IS*, 2018.

[9] S. Saunders and A. Aragón-Zavala, *Antennas and Propagation for Wireless Communication Systems*. Wiley, 2007.

[10] International Commission on Non-Ionizing Radiation Protection, "Guidelines for limiting exposure to electromagnetic fields (100 kHz to 300 GHz)," *Health Phys.*, vol. 118, no. 5, pp. 483–524, 2020.